THE JOURNAL OF PHYSICAL CHEMISTRY B

pubs.acs.org/JPCB Article

Steroidal Molecular Rotors with 1,4-Diethynylphenylene Rotators: Experimental and Theoretical Investigations Toward Seeking Efficient Properties

Karolina Olszewska, Izabella Jastrzebska,* Andrzej Łapiński, Marcin Górecki,* Rosa Santillan, Norberto Farfán, and Tomasz Runka*

Cite This: *J. Phys. Chem. B* 2020, 124, 9625–9635

Read Online

ACCESS | Metrics & More | Article Recommendations | Supporting Information

ABSTRACT: Properly designed molecular rotors with sizable stators and a fast-moving rotator could provide efficient building blocks for amphidynamic crystals. Herein, we report the synthesis of steroidal compounds **1**, **2**, and **3** and their deuterated analogues **1D**, **2D**, and **3D** envisioned to work as molecular rotors. The obtained compounds were characterized by attenuated total reflection-infrared, Raman, and circular dichroism (CD) spectroscopy measurements. The interpretation of spectra was supported by theoretical calculations using density functional theory methods. The analysis of the most characteristic bands confirmed different molecular dynamics of the rotors investigated. Angle-dependent polarized Raman spectra showed the crystallinity of some samples. Electronic CD (ECD) spectra of compounds **1**−**3** and their relevant deuterated analogues **1D**−**3D** are identical. The increase of the band intensity with lowering the temperature shows that the equilibrium is shifted to the thermodynamically most stable conformer. ECD spectra simulated at the TDFFT level of theory for compound **3** were compared with experimental results. It was proved that conformer **3a**, with a torsion angle of +50°, exhibits the best agreement with the experimental results. Simulated vibrational CD and IR spectra for conformer **3a** and its deuterated analogue **3Da** also display good agreement with experimental results. In light of our comprehensive investigations, we evidenced that steroidal compounds **1**, **2**, and **3** can work as molecular rotors.

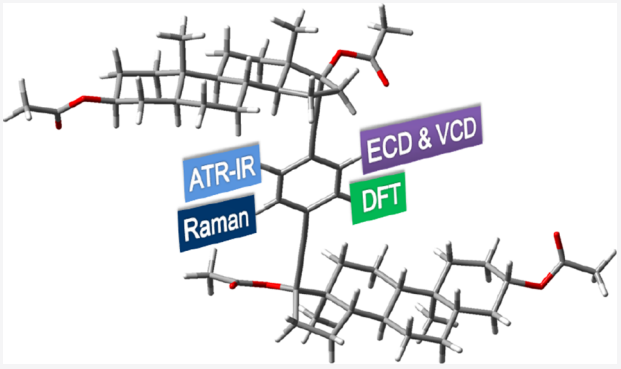

1. INTRODUCTION

In recent years, outlook on how a molecular machine is perceived has changed drastically. In early research, a molecular machine was primarily described as an isolated molecular system, created in the image of molecular motors one can find in a living cell.[1,2] Nowadays, the definition of what a molecular machine is has been extended to include linear,[3] planar,[4] and three-dimensional assemblies. Amid those, solid-state molecular machines are considered as ideal candidates for the development of new functional materials.[5] Furthermore, among crystalline molecular machines, a group of amphidynamic crystals is an especially promising one. By that term, we understand a broad group of molecular crystals that contain highly mobile components inside rigid crystal frames.[6] Those crystals are assemblies of molecules called rotors. A rotor, as shown in Figure 1, consists of three components: the stator, whose role is to create a rigid frame; the rotator, responsible for movement inside the assembly; and the axle of rotation.

As stated by Catalano and Naumov, in order to harness useful functionality, those constructs must fulfill three main design principles.[8] Primarily, they must contain free space around moving components in order to facilitate the

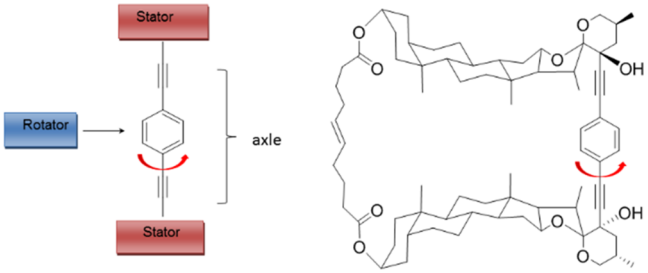

Figure 1. Schematic illustration of the molecular rotor and the structure of the cyclic molecular rotor based on a 1,4-diethynylphenylene rotator.[7]

Received: July 15, 2020
Revised: September 9, 2020
Published: October 16, 2020

movement of the rotator. This can be achieved by numerous means, for example, by introducing massive, steroid-based stators and additional bridging chains connecting them.[7,9] Second, they must contain a volume conserving rotator, which translates into a requirement of high rotational symmetry. Third, the motion of rotators must be correlated. Different amphidynamic crystals that satisfy these conditions can find application in numerous measurement techniques based on the modulation of the rotator rotation because of the interaction with the environment in which the rotor, or crystal, is being placed. Thus, they can find application as molecular sensors,[10] gas storage systems,[11] or gas separation modules.[12] If placed in intracellular surroundings, they can act as viscosity sensors.[13] It has also been shown that they can provide tunable and switchable dielectrics.[14,15]

In this paper, we present the synthesis and vibrational and circular dichroism (CD) spectroscopy characterization of two types of molecular rotors, with steroidal stators and 1,4-diethynylphenylene and 1,4-diethynylphenylene-d_4 groups as a rotator. These compounds were selected based on the similarities and differences between parts of the rotor molecules in order to compare the molecular dynamics and answer the question of which single C−C bond in the rotator is responsible for the rotation (Figure 2). With the conferred spectroscopic study, we will endeavor to solve the problem connected with motion in steroidal molecular rotors.

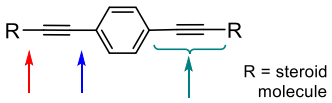

Figure 2. Proposed bonds responsible for rotation in the rotator.

2. MATERIALS AND METHODS

2.1. Synthesis of the Materials. Treatment of steroid **1A** with ethynyl magnesium chloride in dry tetrahydrofuran at 0 °C provided alkyne **1B**. Then, acetylation with Ac_2O in pyridine was performed. Dimers **1** (1,4-bis[17α-ethynyl-5α-androstane-3β,17β-diacetate]-benzene) and **1D** (1,4-bis[17α-ethynyl-5α-androstane-3β,17β-diacetate]-benzene-d_4) were obtained by Sonogashira cross-coupling between alkene **B** and 1,4-diiodobenzene or 2,3,5,6-tetradeuterium-1,4-diiodobenzene in the presence of $Pd(Ph_3)_2Cl_2$, as outlined in Scheme 1. The structure of compound **1** and **1D** was established by ^{1}H, ^{13}C NMR, attenuated total reflection-infrared (ATR-IR), and high-resolution mass spectrometry (HRMS). Compound **2** and **2D** were obtained according to the described protocol.[16] Structures of compounds **2** and **2D** are presented in Figure 3, connected with the motion in steroidal molecular rotors.

Dimer **3** (1,4-bis[4-estren-17α-ethynyl-18a-homo-17β-ol-3-one]-benzene) and **3D** (1,4-bis[4-estren-17α-ethynyl-18a-homo-17β-ol-3-one]-benzene-d_4) were obtained in the same manner as rotors **1** and **1D** (see Scheme 2). Compound **3** was proved to be identical to that described by Santillan et al.[17] The structure of compound **3D** was established by ^{1}H, ^{13}C NMR, ATR-IR, and HRMS.

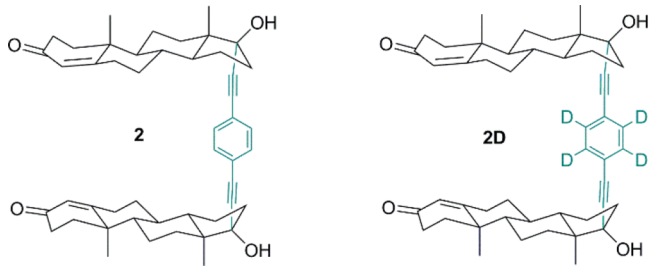

Figure 3. Structures of rotors **2** and **2D**.

2.2. Density Functional Theory Calculations. The dynamics of selected molecular rotors were simulated with the use of Gaussian03[18] and Gaussian16.[19] Density functional theory (DFT) calculations using a B3LYP/6-31G(d) basis set were carried out for an isolated molecule of rotor **3** (Figure 4) on the basis of structural data from the CIF file arising from X-ray analysis reported by Santillan et al.[17] In order to select a molecule for the optimization process, structural data analysis was performed using Olex^2 crystallography software.

This method is a hybrid DFT approach that combines the Becke's three-parameter nonlocal exchange potential with the Lee−Yang−Parr nonlocal correlation functional.[20,21] The frequencies obtained as a result of the calculations were multiplied by a uniform factor of 0.961 in order to eliminate systematic errors related to anharmonicity.[22,23] For the calculation performed, Raman intensity was calculated from scattering activities using the procedure described by Sun et al.[24] The data were calculated for an appropriate temperature of 20 °C and excitation wavelength of 785 nm. The band assignment was performed by the visual inspection of the individual modes with the use of the GaussView 5 program.[25] The input structures for CD study of **3** and **3D** were found by performing conformational searches and the optimizations of the conformers obtained. Final optimizations were run at the B3LYP/6-311+G(d,p) level, including the PCM solvation model for CH_3CN [in the case of electronic CD (ECD)] and $CHCl_3$ [vibrational CD (VCD)] resulted in one stable conformation. Time-dependent-DFT calculations were run with functional CAM-B3LYP and def2-TZVP basis sets, including a PCM for CH_3CN. This selection was inspired based on our previous study on steroid-based compounds.[26−29] All spectra were generated using the program SpecDis.[30]

2.3. ATR-IR Spectroscopy. A Bruker Equinox 55 FTIR spectrometer equipped with a Gateway 6 reflection horizontal

Scheme 1. Synthesis of Rotors 1 and 1D

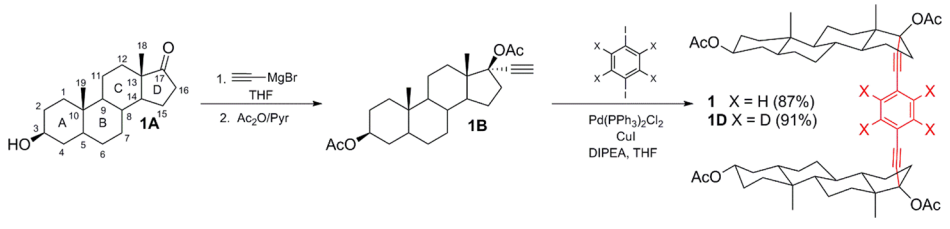

https://dx.doi.org/10.1021/acs.jpcb.0c06464
J. Phys. Chem. B 2020, 124, 9625−9635

Scheme 2. Synthesis of Dimer 3 and 3D

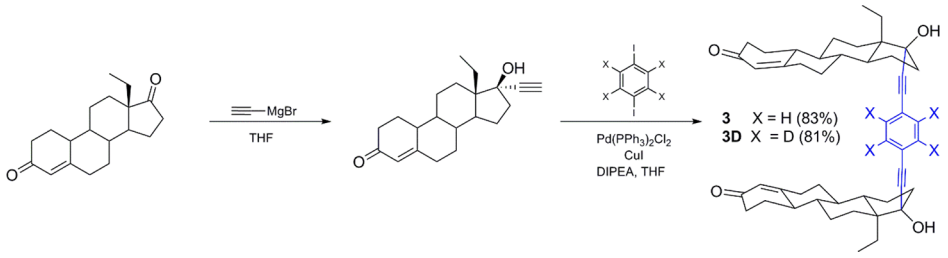

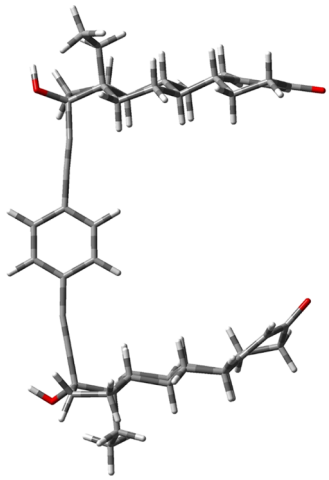

Figure 4. Model of the molecule of rotor **3**.[17]

ATR system, a deuterated triglycine sulfate detector, and a KBr beam splitter was used for spectral acquisition. The ATR accessory consisted of an optical unit and a top plate assembly with a 45° angle zinc selenide (ZnSe) crystal that allowed the measurement of liquids and solids. All spectra were recorded in the range of 4000−600 cm^{-1} using the ATR method with a resolution of 2 cm^{-1} and 2500 scans.

2.4. Raman Spectroscopy. The Raman spectra of nonoriented samples of molecular rotors **1**, **2**, and **3** and deuterated **1D**, **2D**, and **3D** compounds were recorded using a Renishaw inVia Raman microscope equipped with a thermoelectrically—cooled charge-coupled device detector and near IR laser working at 785 nm wavelengths. The Raman spectra were recorded in the spectral range 100−3200 cm^{-1} with a spectral resolution better than 2 cm^{-1}. To avoid sample overheating, the power of the laser beam was kept below 10 mW. The position of Raman peaks was calibrated before collecting the data using a crystalline silicon sample as an internal standard. The spectral parameters of the bands were determined using the fitting package of Wire 3.4 software.

2.5. CD Spectroscopy. All experimental ECD spectra were carried out using a J-815 spectrometer (Jasco, Tokyo, Japan) at room temperature in spectroscopic grade CH_3CN in a quartz cell with path lengths of 1 and 0.1 cm for a solution with a concentration of 0.28−0.30 mM. All spectra were measured using a scanning speed of 100 nm min^{-1}, a step size of 0.2 nm, a band width of 2 nm, and accumulation of five scans. The spectra were background-corrected using spectra of solvents. Additionally, for compound **3**, variable-temperature ECD measurements were carried out by using an Optistat optical spectroscopy cryostat (Oxford Instruments, Abingdon, UK) fixed to the sample compartment of the ECD instrument, in the temperature range from +25 to −160 °C, using the same measurement parameters. Baseline correction was done by subtracting the spectrum of a reference solvent obtained under the same conditions; the normalization was done using a concentration at 25 °C. The VCD and IR spectra of **3** and **3D** were measured simultaneously using a Chiral IR-2X from BioTools (Jupiter, FL, USA) at a resolution of 4 cm^{-1} in the range of 2000−950 cm^{-1} in $CDCl_3$ as a solvent. A solution with a concentration of ∼0.1 M was measured in a BaF_2 cell

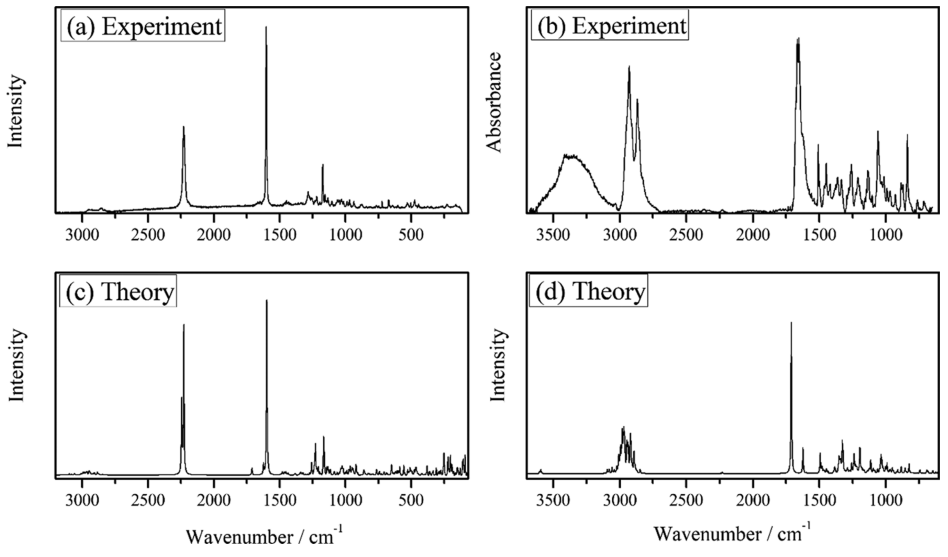

Figure 5. Experimental and theoretical (scaling factor = 0.961) spectra of rotor **3**: Raman (a,c) and IR (b,d).

https://dx.doi.org/10.1021/acs.jpcb.0c06464
J. Phys. Chem. B 2020, 124, 9625−9635

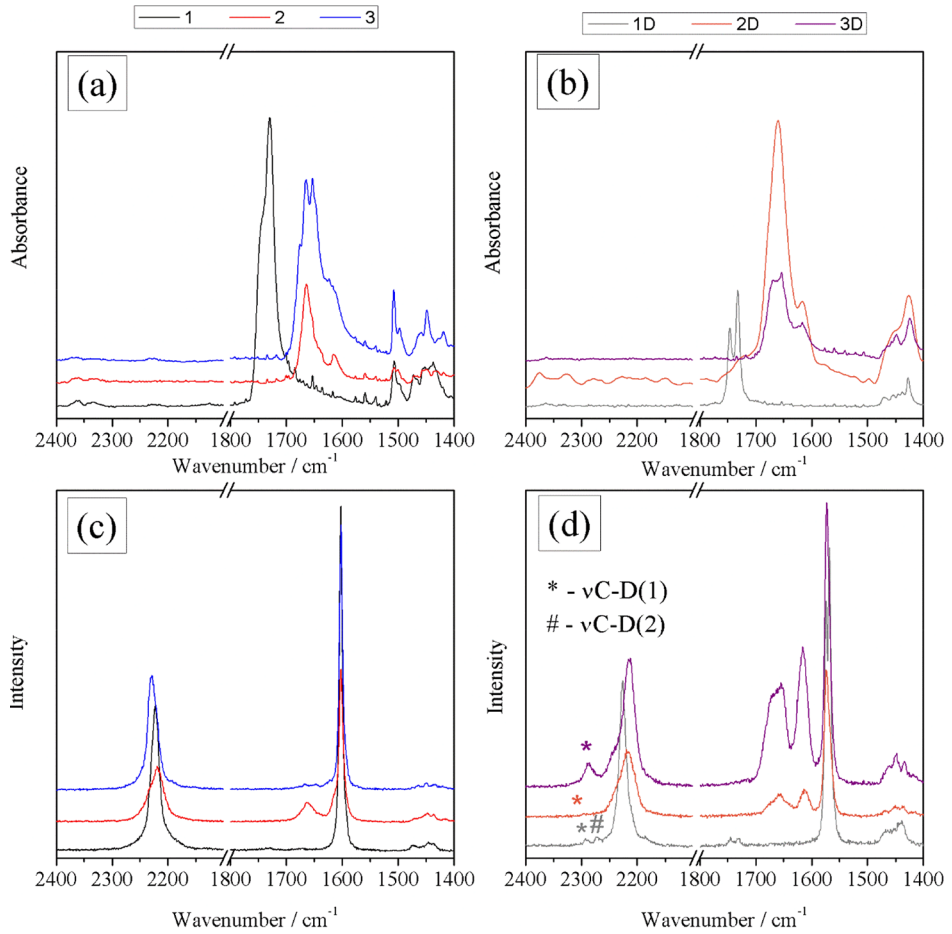

Figure 6. ATR-IR (a,b) and Raman (c,d) spectra of non-deuterated and deuterated compounds. Bands * and # are assigned to stretching vibrations of C−D bonds.

Table 1. Positions (cm^{-1}) of Bands in the Raman and ATR-IR Spectra of Rotors 1−3 and 1D−3D in the 2300−1400 cm^{-1} Range and Proposed Assignment[a]

rotor **1**		rotor **2**		rotor **3**		rotor **1D**		rotor **2D**		rotor **3D**		
Raman	IR-ATR	Raman	IR-ATR	Raman	IR-ATR	Raman	IR-ATR	Raman	IR-ATR	Raman	IR-ATR	interpretation
						2291 w		2289 w		2287 w		ν C−D (R)
						2270 w						
		2234 m		2230 w		2226 s		2240 w		2243 w		ν C≡C
2223 s		2219 s		2220 s		2210 w		2216 s		2215 s		
1746 w	1746 m					1744 w	1746 s					ν C═O (S)
1727 w	1729 s					1731 w	1732 s					
			1684 w	1683 w								ν C═O (S)
					1677 s			1674 w	1673 s	1672 s	1671 s	
		1662 m	1665 s	1666 w	1666 s				1659 v			
			1656 s		1653 s			1654 m	1654 m	1653 s	1653 s	
			1639 m	1647 w					1623 w			
		1614 m	1613 m	1623 w	1622 m			1613 m	1611 m	1616 s	1617 s	ν C═C (S)
1603 s		1603 s		1603 s		1575 s		1574 s		1574 s		ν C═C (R)
1596 w		1597 m		1593 s		1568 s		1567 s		1570 s		
						1559 w						
	1507 w		1508 w		1508 s		1426 m		1424 m		1424 s	
	1497 w		1500 w		1498 w							

[a]Abbreviations: s—strong, m—medium, w—weak, R—rotator, S—stator.

with a path length of 100 μm over the course of ca. 8 h to improve the signal-to-noise ratio. Baseline correction was achieved by subtracting the spectrum of a solvent recorded under the same conditions.

https://dx.doi.org/10.1021/acs.jpcb.0c06464
J. Phys. Chem. B 2020, 124, 9625−9635

3. RESULTS AND DISCUSSION

3.1. Characterization of the Materials. *ATR-IR and Raman Spectroscopy*. Three compounds named rotors **1**, **2**, and **3** and their deuterated analogues **1D**, **2D**, and **3D** were chosen for vibrational spectroscopy characterization. Raman and ATR-IR spectroscopy methods were used, and the experimental results were verified by theoretical calculations using the B3LYP/6-31G(d) method. The theoretical calculations were performed for molecules of rotor **3**, for which the crystallographic structure has been published.[17] The calculated and experimental Raman and IR spectra of rotor **3** are shown in Figure 5. Moreover, all calculated wavenumbers, activity in Raman and IR spectra, and proposed assignment are presented in Table S1 in the Supporting Information.

The spectra consist of many bands, so for the analysis and assignment of modes, and will be divided into subranges. In the ATR-IR spectra of **2**, **2D**, **3**, and **3D**, broadbands observed in the range 3500−3010 cm^{-1} are assigned to stretching vibrations of O−H bonds (Figure S1 in Supporting Information). In the range between 3050 and 2800 cm^{-1} in both Raman and ATR-IR spectra, multicomponent bands assigned to symmetric and antisymmetric stretching vibrations of saturated C−H bonds are recorded for all compounds. The above observation is confirmed by theoretical calculations.

The Raman and ATR-IR spectra of non-deuterated **1**, **2**, and **3** and deuterated **1D**, **2D**, and **3D** rotors in the region of the rotator vibrations are presented in Figure 6. In the range from 2400 to 1400 cm^{-1}, bands of the highest intensity both in Raman and ATR-IR spectra are observed. Most of these bands are assigned to the different vibrations of a rotator, and the axle of rotation and this range is of particular interest. In Table 1, wavenumbers and the assignment of these bands are provided. A medium intensity band located above 2200 cm^{-1} in Raman spectra of both non-deuterated and deuterated rotors is assigned to the stretching vibrations of C≡C bonds that form the axle of rotation. The position and intensity of the band vary for different rotors. In the Raman spectrum of rotor **1**, a singular band with a peak located at 2223 cm^{-1} is observed. In the Raman spectra of a deuterated analogue **1D**, the band consists of two components; the main is located at 2226 cm^{-1} and a weaker band, in the form of asymmetry of main band, at 2210 cm^{-1}. The opposite behavior can be perceived in the spectra gathered for the pairs of rotors **2** and **2D** and **3** and **3D**. For all of them, the band under discussion consists of two components with the less intense one shifted to higher wavenumbers. Comparing the positions, one can notice a red shift of the main component and a blue shift of a secondary component in the spectra of deuterated rotors **2D** and **3D**, in relation to the spectra of rotors **2** and **3**. The analysis of ATR-IR spectra indicates a lack of the bands in the spectral region discussed. Theoretical spectra confirm this observation (see Figure 5). The interpretation of the experimental observations discussed above leads to several essential remarks. Similar values of wavenumbers of the main band attributed to C≡C bonds for the pairs of rotors **2** and **3** and also for **2D** and **3D** indicate a similar chemical environment of the rotators in pairs of molecules (non-deuterated and deuterated). This indicates that an additional ethyl group present in rotors **3** and **3D** does not influence the rotational dynamics of the rotator. The decrease in the wavenumber of this band for pairs of rotors **2** (2219 cm^{-1}) and **2D** (2216 cm^{-1}) and **3** (2220 cm^{-1}) and **3D** (2215 cm^{-1}) can be explained with mass effect. A deuterated rotator in **2D** and **3D** has a more substantial mass, and thus, a higher moment of inertia, which causes a more significant deformation of the rotating ring (it flattens in the direction of the rotation axis). This leads to a slight elongation of the C≡C bonds and then, due to the smaller value of bond force constant, the wavenumber of the band assigned to the stretching vibration of the C≡C bonds shifts to lower wavenumber values. However, the wavenumber of the stretching vibration of C≡C bonds for rotors **1** and **1D** is greater than for the rest of rotors because the steric hindrance for ring rotation is larger because of the existence of acetate groups in the proximity of the rotating ring. As a consequence, the frequency of rotator rotation decreases and causes smaller, compared to rotors **2**, **2D**, **3**, **3D**, ring deformation. As a result, the length of C≡C bonds in rotors **1** and **1D** is slightly shorter, the force constant is greater, which leads to the higher wavenumber of bands corresponding to stretching vibrations of C≡C bonds being observed. However, there are no bands present in the experimental ATR-IR spectra of all rotors (non-deuterated and deuterated) assigned to the stretching vibrations of C≡C bonds. This is in agreement with the theoretical calculations that indicate practically negligible intensity of this vibration in the IR spectrum (see Figure 5).

In the Raman spectra of rotors **1D**, **2D**, and **3D**, bands assigned to the stretching vibrations of C−D bonds are revealed in the slope of the band assigned to the C≡C stretch, on the higher energy side of the band. Two bands are present for rotor **1D**, and a singular band is observed for rotors **2D** and **3D**. All the bands assigned to the stretching vibrations of C−D bonds are recorded with very low intensity.

In the spectral range 1680−1620 cm^{-1}, in the Raman and ATR-IR spectra of rotors **2**, **2D**, **3**, and **3D**, multicomponent bands are recorded that can be assigned to the in-phase and out-of-phase stretching vibrations of C═O bonds occurring in rings A of the stators. For rotor **2D** and **3D**, bands present in the Raman spectra are of higher intensity compared to the analogous bands present in the Raman spectra of rotors **2** and **3**. For rotors **1** and **1D**, the ester carbonyl group stretching vibrations are observed as two peaks in the range between 1750 and 1720 cm^{-1}, strong in the ATR-IR spectra and very weak in the Raman spectra. A substantial difference in the position of bands attributed to the C═O stretching vibration between rotors **1** and **1D** and **2**, **2D**, **3**, and **3D** is related to the location of the group in the rotor molecule. As it is seen from Schemes 1 and 2 and Figure 3 for rotors **1** and **1D**, the acetate groups are present at C17 in ring D, while in the case of rotors **2**, **2D**, **3**, and **3D**, there are α,β-unsaturated carbonyl C═O groups (A ring). It is worth to note that carbonyl bonds are highly polar because of the large electronegativity between carbon and oxygen. This generates a significant dipole moment and, as a result, provides an intense band that corresponds to the stretching vibration in the IR spectrum (usually very weak in the Raman spectrum). Generally, the band assigned to stretching vibrations of α,β-unsaturated carbonyl groups is registered at much lower wavenumbers in vibrational spectra, as compared to the C═O bond stretch in acetate groups. This is because the α,β-unsaturated carbonyl group is conjugated with a carbon−carbon double bond. This causes the C═O bond to weaken, lowers the force constant, and, hence, shifts the band position of stretching vibration toward lower wavenumbers. The analysis of our results indicates a difference of about 80 cm^{-1}. Additionally, this promotes geometrical changes and, in consequence, increases the activity of the

https://dx.doi.org/10.1021/acs.jpcb.0c06464
J. Phys. Chem. B 2020, 124, 9625−9635

stretching vibration of C═O bonds in Raman spectra of rotors **2**, **2D**, **3**, and **3D**, as compared to **1** and **1D**. Moreover, for deuterated compounds **2D** and **3D**, the increase in the intensity of the C═O vibration, in Raman spectra with respect to non-deuterated compounds, **2** and **3**, can be caused by changes in the rotational dynamics of the rotator and the influence on α,β-unsaturated carbonyl groups in stators. For the asymmetric stretching vibration of the C═C bond in the aromatic ring of the rotator, a two-component band near 1600 cm^{-1} and a two-component band near 1500 cm^{-1} are present, respectively, in the Raman and the ATR-IR spectra of rotors **1**, **2**, and **3**. The positions of the bands in the corresponding spectra of rotors **1D**, **2D**, and **3D** are shifted toward lower wavenumbers. This is confirmed by theoretical calculations conducted for rotor **3**, according to which there are two different stretching vibrations of double C═C bonds present in the rotator, one at 1597 cm^{-1}, with high intensity in Raman spectroscopy, and a second one at 1493 cm^{-1} of medium intensity in an IR spectrum.

In the experimental spectra of rotors **2**, **2D**, **3**, and **3D**, there is also an additional asymmetric band in the 1620−1610 cm^{-1} range, originating from the stretching vibration of C═C bonds present in the A ring of the stators mentioned above. In the range between 1450 and 1400 cm^{-1}, in both Raman and ATR-IR spectroscopy, multicomponent bands are recorded. Bands in this region can be assigned to scissoring vibrations of methyl and methylene groups that are also present in the stators.

The observation of crystallite morphology of all samples under an optical microscope allows us to select those for further spectroscopic characterization. Samples of rotors **1**, **3**, and **3D** are the most interesting for further measurements because of their well-shaped crystallites of size ranging from a couple of microns, in the case of rotor **1**, to several hundred microns, in the case of rotor **3D**. Rotors **2** and **2D** present as very fine powders, with particles of sizes distinctly below micrometer. Here, we show the results of the spectroscopic study concerning polarized Raman spectra measurements and angular analysis for rotors **1**, **3**, and **3D**. For each of the rotors, one crystallite with a well-developed crystalline surface was chosen for the measurements of polarized Raman spectra.

The polarized Raman spectra of the selected crystallites of rotors **1**, **3**, and **3D** are presented in Figure 7. In all cases, spectra show significant changes in the intensity of the bands for parallel (XX) and cross (XY) polarization, which indicates the crystallinity of the sample. The comparison of the polarized spectra for all other rotors are depicted in Figure S2 (Supporting Information). As it is seen from Figure 7a−c, the intensity of modes assigned to the stretching vibration of the C≡C bond in the axle and C═C bonds in the ring of the rotator for parallel (XX) and perpendicular (XY) polarization is very different, that is, from about three to five times higher in (XX) polarization, whereas the intensity of other modes assigned to C═O, C═C (S) in stators, O−H or skeletal, and C−D bonds (the last one only for deuterated compound) is comparable for both polarizations. The relation between the intensity of the bands mentioned above reverses after rotating the samples by an angle of 90° (see Figure S3 in Supporting Information). This is a consequence of the change in selection rules for crystalline materials. In the discussed spectral range of Raman spectra, it can be seen that the intensity of the bands depends on the geometrical relationship between the polarization of the incident laser light (direction of the electric field vector) and the orientation of the rotor molecule. For a 0° angle, the electric field vector of the incident laser light must be parallel or almost parallel to the axle of the rotator in the rotor molecule, that is, parallel to C≡C bonds, resulting in the maximum intensity of the band assigned to C≡C bond stretch. For an angle of a 90°, the electric field vector is

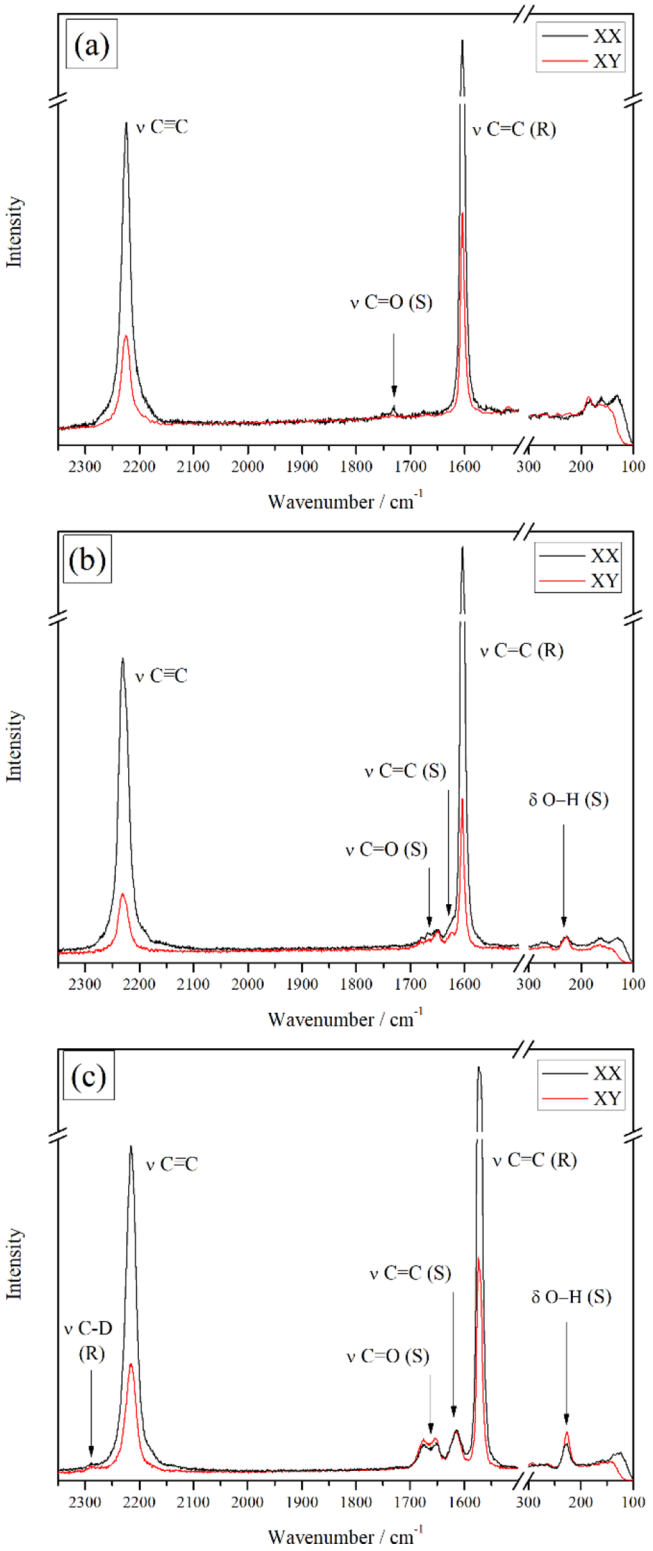

Figure 7. Selected parts of the Raman spectrum associated with vibrations of double and triple CC bonds, carbonyl groups, C−D, and O−H for rotors **1** (a), **3** (b), and **3D** (c) are presented. R—rotator, S—stator.

https://dx.doi.org/10.1021/acs.jpcb.0c06464
J. Phys. Chem. B 2020, 124, 9625−9635

perpendicular to the axle, and so the vibration observed cannot be excited, resulting in the disappearance of the latter band. For a rough analysis of the spectroscopic results of crystalline samples, let us now assume that the stators are perpendicular to the axle. Then, for an angle of 90°, the electric field vector of incident light is parallel to the stators. Thus, the electric field vector is close to parallel to C═O and O−H bonds for rotors **3** and **3D**. The intensity of the bands assigned to the vibrations of these bonds would be then maximum. We should note that there are no bands corresponding to such bonds (C═O and O−H) in the spectrum of rotor **1**.

In the abovementioned approximation, we roughly assumed the right-angle geometry of the rotor molecule and also that the molecule lies in the plane of observation. Given that the bands in the spectra appear as not quite polarized, this assumption may not be entirely correct for a real crystal. The geometry of rotor molecule **3** drawn on the basis of crystallographic data (Figure 4) indicates that the angle between stators and axle of rotator is slightly different than 90°. Additionally, the angular dependence of the intensity of stretching vibrations of C−D bonds is similar to that of C═O and O−H bonds (**3D**), which confirms a similar geometrical orientation of these three bonds in the molecule. To further investigate the polarization differences, the measurements of samples of rotors **1**, **3**, and **3D** were carried out for different angles while the crystallite was rotated by a predetermined angle. Figures 8a and 9a show the dependence of the intensity

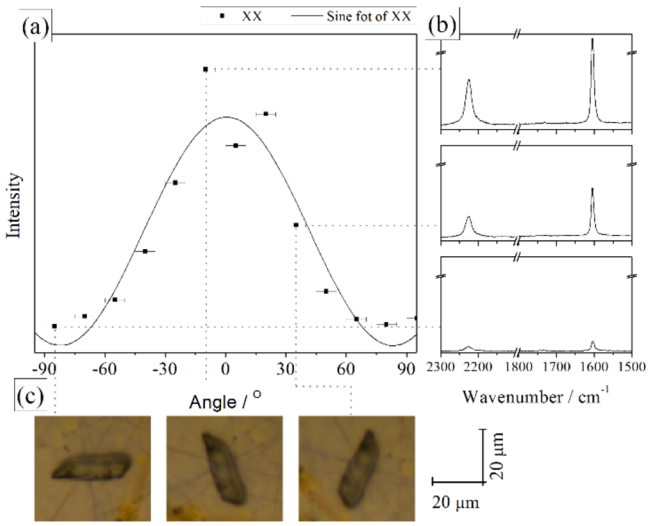

Figure 8. Dependencies of intensity vs angle of rotation of the sample for the band assigned to stretching vibration of C═C bonds in the rotator recorded in parallel (XX) polarization for rotor **1**. The Raman spectra recorded for corresponding angles are depicted on the right side.

recorded in parallel (XX) polarization versus angle of rotation of the samples **1** and **3** for the mode assigned to the stretching vibration of the C≡C bond in the rotator. The dependence for sample 3D is shown in Figure S4 in Supporting Information. For all crystallites measured, the initial orientation was not only different but also impossible to determine in the midst of conducting measurement. Therefore, the maximum intensity can be observed for different angles. On that account, the scale of angles, as shown in Figures 8a, 9a, and S4, was adjusted so that an angle of 0° would match the maximum of the Raman signal calculated from the sine

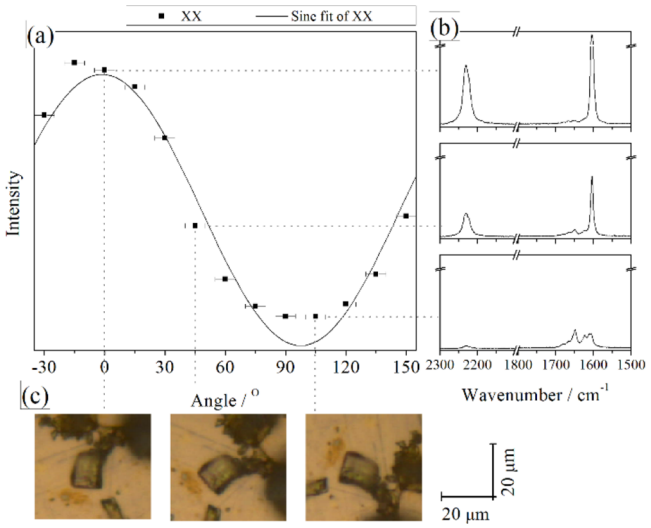

Figure 9. Dependencies of intensity vs angle of rotation of the sample for the band assigned to stretching vibration of C═C bonds in rotator recorded in parallel (XX) polarization for rotor **3**. The Raman spectra recorded for corresponding angles are depicted on the right side.

approximation of the dependences measured. Experimental dependences for all samples were fitted using the sine function

$$y = y_0 + A \sin\left(\pi \frac{x - x_C}{w}\right) \quad (1)$$

The maximum and minimum of the Raman signal are separated by an angle of about 90°. The Raman spectra that correspond to three different angular positions of the samples are depicted in Figures 8b and 9b. Tracking the dotted lines from the Raman spectra to the bottom part of the figures, one can see the assignment of corresponding spectra to the angular position of the crystal investigated (Figures 8c and 9c).

3.2. CD Analysis. CD spectroscopy has constantly illustrated its high sensitivity in the study of conformational diversity of chiral species, as well as their conformational stability.[26,31−37] Therefore, in the course of this work, we decided to add this technique to our in-depth studies to explore the ECD and VCD properties in order to gain more insights into the conformational stability in solution of the investigated steroidal rotors. First, ECD and UV spectra of **1**−**3** and **1D**−**3D** were recorded in acetonitrile at room temperature (Figure 10). The ECD curves exhibit two types of profiles, which are significantly different from each other in the position of Cotton effects (CEs) and their intensity. In all cases, ECD spectra of steroidal compounds **1**−**3** and their relevant deuterated analogues **1D**−**3D** are identical. The replacement of hydrogen with deuterium is not expected to have any effect on the ECD spectra, and this effect is also quite minor on the presented VCD spectra because of the great flexibility of the axle, as well as the rotator. The experimental data of **1** and **1D** display one negative CE at 275 nm and shoulders at 250, 220, and 210 nm. These bands are mainly attributed to $\pi-\pi^*$ transitions of the diethynylphenylene chromophore. In the same region in the UV spectrum, there are bands at ∼325, 290, 270, 220, and 213 nm. For rotors **2** and **3** and **2D** and **3D**, there is a broad long-wavelength negative CE centered at ∼330 nm related to the $n-\pi^*$ transition of the enone chromophore in the stator part of molecule, then there are two intense bands centered at ∼240

https://dx.doi.org/10.1021/acs.jpcb.0c06464
J. Phys. Chem. B 2020, 124, 9625−9635

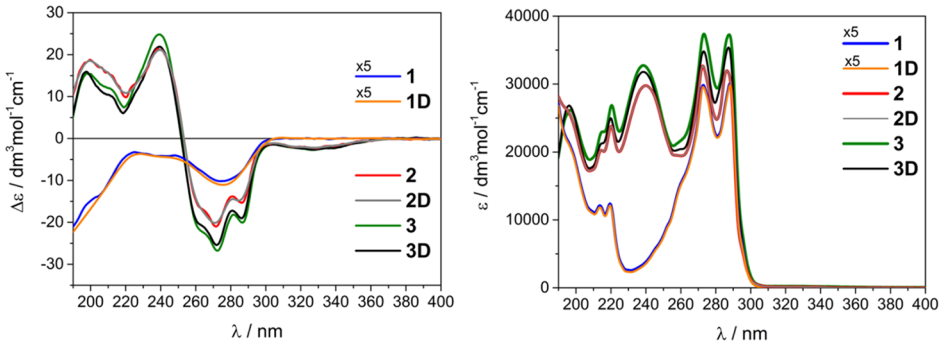

Figure 10. ECD and UV spectra of **1**−**3** and **1D**−**3D** rotators measured in acetonitrile at room temperature.

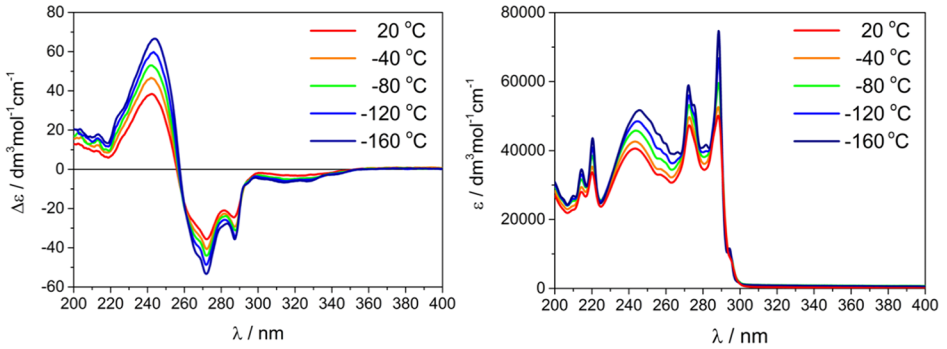

Figure 11. Variable low-temperature ECD and UV measurements of **3** recorded in the mixture of MeOH/EtOH = 1:4.

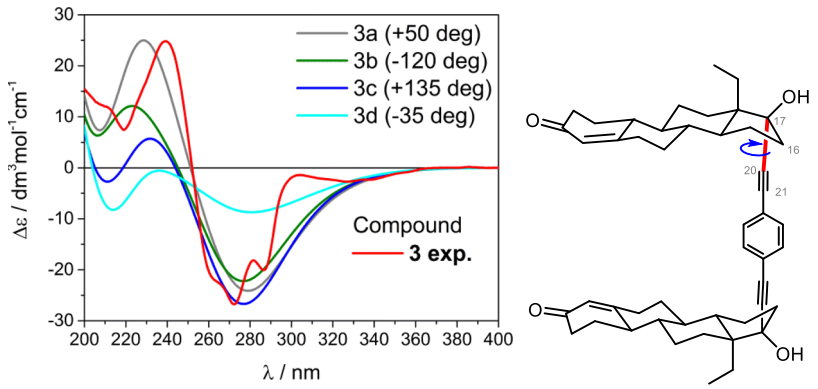

Figure 12. Comparison of the experimental and simulated spectra of **3** by changing the torsion angle C16−C17−C20−C21 (band width = 0.43 eV, UV shift = 0 nm).

nm derived from $\pi-\pi^*$ benzene transitions, and a band at ∼215 nm originating from admixture of the $\pi-\pi^*$ benzene and enone transitions. However, because of the slight energy difference between these excitations their precise determination is impeded. One may also notice that the CE centered at 270 nm exhibits a well-developed vibrational structure.

Next, in the course of our work, the variable low-temperature ECD measurements were carried out to check the thermal stability of the investigated molecular rotors. As a model for this part of the study, we selected rotor **3**. In Figure 11, the ECD spectra recorded in the mixture MeOH/EtOH = 1:4 in the temperature range from +20 to −160 °C are shown. As shown in Figure 11, lowering the measurement temperature resulted in a substantial change in the intensity of all ECD/UV bands, with the two isodichroic points at 260 and 291 nm. The ECD spectra showed a systematic increase of band intensity with lowering the temperature. This means that the equilibrium is shifted to the thermodynamically most stable conformer. The changes in the intensity of the main bands are because of the flexibility of the bonds throughout the entire rotator bridge, while the steroid part remains stable. This hypothesis is supported by the fact that steroidal stators are quite conformationally rigid and do not generate any significant impact onto the variable-temperature ECD spectra.

In order to predict the most favorable conformation(s) in solution, we simulated at the TDFFT level of theory ECD spectra for representative conformers of rotor **3** by changing systematically the torsion angle C16−C17−C20−C21 (acc. numbering in Scheme 1 and Figure 12), starting directly from the modification of the X-ray structure previously published for a similar compound.[16] We used this strategy because computed conformers (obtained by simulations using molecular mechanics level follow by DFT optimizations) exhibit plenty of structures with quite similar energy differences (Figure S5). This approach is based on the straight comparison of experimental and simulated spectra: a good match supports

https://dx.doi.org/10.1021/acs.jpcb.0c06464
J. Phys. Chem. B 2020, 124, 9625−9635

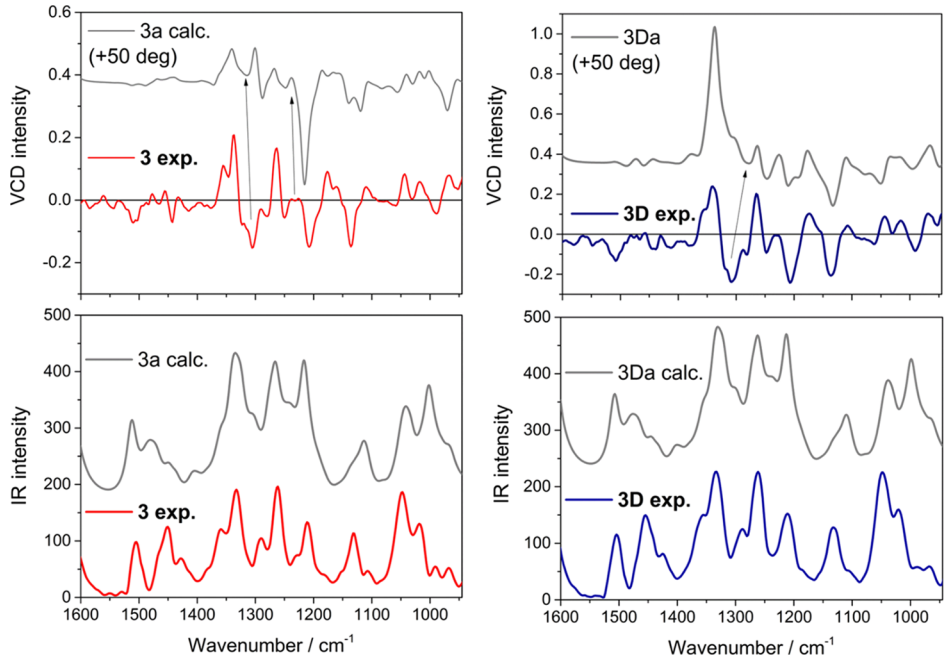

Figure 13. Comparison of the experimental and calculated VCD and IR spectra of **3** and **3D** (band width = 10 cm^{-1}, scaling factor = 0.983).

the predicted conformational analysis.[38] For all conformers, ECD spectra were calculated at the CAM-B3LYP/def2-TZVP level of theory using the PCM model for CH_3CN. As a result of our analysis, conformer **3a** with the value of torsion angle +50° shows the most intense CEs at ca. 230 nm. Thus, this conformation exhibits the best agreement with the experimental data (Figure 12), actually indicating the most stable structure in solution among the set of investigated structures. Some inconsistency in the range 300−380 nm are related to the use of a constant band width for the whole investigated spectral region (see also Figure S6). Another way of looking at the question of conformational stability is VCD spectroscopy. The experimental VCD and IR spectra of **3** and **3D** are recorded in chloroform and presented in Figure 13, together with DFT simulations performed for previously selected conformation **3a** and **3Da** at the B3LYP/6-311+G(d,p) level of theory using the PCM model for $CHCl_3$.

DFT simulations for **3a** and its deuterated analogue **3Da** show good agreement with the experimental spectra; all experimental spectral features are well reproduced. This additionally confirms the validity of the computed conformational species and conclusions derived from ECD on the most preferable conformation in solution.

4. CONCLUSIONS

The comprehensive spectroscopy analysis of molecular rotors **1**−**3** and their deuterated analogues **1D**−**3D** was performed. The interpretation of the experimental data was supported by quantum chemical calculations. Vibrational spectroscopy provided information which allows to distinguish structures of rotors, mainly due to the differences between functional groups in stators and deuterated rotator. The analysis of the most characteristic bands confirmed different molecular dynamics of the rotors investigated. However, there is no spectroscopic evidence as to which single C−C bond is responsible for the rotation of the rotator. Angle-dependent polarized Raman spectra confirmed the crystallinity of three samples. ECD and VCD spectra of compounds **1**−**3** and their relevant deuterated analogues are identical because there is no any influence of deuterium substitution onto the electronic transitions of chromophore units. Furthermore, this influence is also not visible in vibrational spectra perhaps because of the great flexibility of the axle, as well as the rotator. The thermal stability monitored by the low-temperature ECD measurements shows that the equilibrium is shifted to the thermodynamically most stable conformer. This finding was fully confirmed by theoretical simulations of chiroptical data. On the other hand, calculations of ECD and VCD data and their good reproduction proved that the investigated rotors exhibit properties which are not governed by supramolecular interaction. In light of our experimental results supported by theoretical calculations, we are able to probe the vibrational, optical, and chiroptical properties of steroidal compounds and confirm that they can work as molecular rotors.

■ ASSOCIATED CONTENT

Supporting Information

The Supporting Information is available free of charge at https://pubs.acs.org/doi/10.1021/acs.jpcb.0c06464.

Synthesis details for **1**, **1D**, and **3D** compounds (^1H, ^{13}C NMR, and HRMS), results of DFT calculation for the model of rotor **3**, ATR-IR spectra of rotors **2**, **2D**, **3**, and **3D**, polarized Raman spectra of rotors **1**, **2**, and **2D**, polarized Raman spectra of rotors **1D**, **3**, and **3D** after rotating the sample by 90°, simulated spectrum of **3a** and steroidal unit at the CAM-B3LYP/def2-TZVP/PCM(CH_3CN) level of theory, and overview of conformational search for compounds **3** carried out at the B3LYP/6-31G(d) level of theory (PDF)

■ AUTHOR INFORMATION

Corresponding Authors

Izabella Jastrzebska − *Faculty of Chemistry, University of Białystok, 15-254 Białystok, Poland*; Phone: +48 85 738 80 43; Email: i.jastrzebska@uwb.edu.pl

https://dx.doi.org/10.1021/acs.jpcb.0c06464
J. Phys. Chem. B 2020, 124, 9625−9635

Marcin Górecki − *Institute of Organic Chemistry, Polish Academy of Sciences, 01-224 Warsaw, Poland;* orcid.org/0000-0001-7472-3875; Phone: +48 22 343 20 00; Email: marcin.gorecki@icho.edu.pl

Tomasz Runka − *Faculty of Materials Engineering and Technical Physics, Poznan University of Technology, 60-965 Poznań, Poland;* orcid.org/0000-0002-0965-2676; Phone: +48 61 665 31 55; Email: tomasz.runka@put.poznan

Authors

Karolina Olszewska − *Faculty of Materials Engineering and Technical Physics, Poznan University of Technology, 60-965 Poznań, Poland*

Andrzej Łapiński − *Institute of Molecular Physics, Polish Academy of Sciences, 60-179 Poznań, Poland*

Rosa Santillan − *Departamento de Química, Centro de Investigación y de Estudios Avanzados del IPN, México D.F. 07000, Mexico*

Norberto Farfán − *Facultad de Química, Departamento de Química Orgánica, Universidad Nacional Autónoma de México, 04510 Ciudad de México D.F., Mexico*

Complete contact information is available at: https://pubs.acs.org/10.1021/acs.jpcb.0c06464

Author Contributions

The manuscript was written through contributions of all the authors. All the authors have given approval to the final version of the manuscript.

Notes

The authors declare no competing financial interest.

■ ACKNOWLEDGMENTS

This work was partially supported by the Ministry of Science and Higher Education. M.G. thanks the Wroclaw Centre for Networking and Supercomputing (WCSS) for the computational support. N.F. and R.S. acknowledge support from PAPIIT (IN222819), DGAPA and CONACyT.

■ REFERENCES

(1) Schliwa, M.; Woehlke, G. Molecular motors. *Nature* **2003**, *422*, 759−765.

(2) Bucci, E. M.; Bucci, O. M.; Sorrentino, R. Nanotechnology and Life: An Engineer's Perspective [Point of View]. *Proc. IEEE* **2014**, *102*, 930−935.

(3) Liu, Y.; Flood, A. H.; Bonvallet, P. A.; Vignon, S. A.; Northrop, B. H.; Tseng, H.-R.; Jeppesen, J. O.; Huang, T. J.; Brough, B.; Baller, M.; Magonov, S.; Solares, S. D.; Goddard, W. A.; Ho, C.-M.; Stoddart, J. F. Linear Artificial Molecular Muscles. *J. Am. Chem. Soc.* **2005**, *127*, 9745−9759.

(4) Eelkema, R.; Pollard, M. M.; Vicario, J.; Katsonis, N.; Ramon, B. S.; Bastiaansen, C. W. M.; Broer, D. J.; Feringa, B. L. Nanomotor rotates microscale objects. *Nature* **2006**, *440*, 163.

(5) Garcia-Garibay, M. A. Crystalline molecular machines: Encoding supramolecular dynamics into molecular structure. *Proc. Natl. Acad. Sci. U. S. A.* **2005**, *102*, 10771−10776.

(6) Karlen, S. D.; Garcia-Garibay, M. A. Amphidynamic Crystals: Structural Blueprints for Molecular Machines. In *Molecular Machines. Topics in Current Chemistry*; Kelly, T. R., Ed.; Springer-Verlag Berlin Heidelberg, 2005; Vol. *262*, pp 179−227.

(7) Czajkowska-Szczykowska, D.; Jastrzebska, I.; Santillan, R.; Morzycki, J. W. The synthesis of disteroidal macrocyclic molecular rotors by an RCM approach. *Tetrahedron* **2014**, *70*, 9427−9435.

(8) Catalano, L.; Naumov, P. Exploiting rotational motion in molecular crystals. *CrystEngComm* **2018**, *20*, 5872−5883.

(9) Runka, T.; Olszewska, K.; Fertsch, P.; Łapiński, A.; Jastrzebska, I.; Santillan, R.; Farfán, N. Vibrational spectroscopic characterization of cyclic and acyclic molecular rotors with 1,4-diethynylphenylene-d4 rotators. *Spectrochim. Acta, Part A* **2018**, *192*, 393−400.

(10) Mu, X.; Liu, Y.; Liu, S.; Sun, Y.; Lu, N.; Lu, Y.; Li, W.; Zhou, X.; Liu, B.; Li, Z. A cyanine-derived near-infrared molecular rotor for ratiometric imaging of mitochondrial viscosity in cells. *Sens. Actuators, B* **2019**, *298*, 126831−126839.

(11) Aguilar-Granda, A.; Pérez-Estrada, S.; Sánchez-González, E.; Álvarez, J. R.; Rodríguez-Hernández, J.; Rodríguez, M.; Roa, A. E.; Hernández-Ortega, S.; Ibarra, I. A.; Rodríguez-Molina, B. Transient Porosity in Densely Packed Crystalline Carbazole-(p-Diethynylphenylene)-Carbazole Rotors: CO_2 and Acetone Sorption Properties. *J. Am. Chem. Soc.* **2017**, *139*, 7549−7557.

(12) Metrangolo, P.; Carcenac, Y.; Lahtinen, M.; Pilati, T.; Rissanen, K.; Vij, A.; Resnati, G. Nonporous Organic Solids Capable of Dynamically Resolving Mixtures of Diiodoperfluoroalkanes. *Science* **2009**, *323*, 1461−1464.

(13) Aguilar-Granda, A.; Pérez-Estrada, S.; Roa, A. E.; Rodríguez-Hernández, J.; Hernández-Ortega, S.; Rodriguez, M.; Rodríguez-Molina, B. Synthesis of a Carbazole-[pi]-carbazole Molecular Rotor with Fast Solid State Intramolecular Dynamics and Crystallization-Induced Emission. *Cryst. Growth Des.* **2016**, *16*, 3435−3442.

(14) Zhang, W.; Ye, H.-Y.; Graf, R.; Spiess, H. W.; Yao, Y.-F.; Zhu, R.-Q.; Xiong, R.-G. Tunable and Switchable Dielectric Constant in an Amphidynamic Crystal. *J. Am. Chem. Soc.* **2013**, *135*, 5230−5233.

(15) Kobr, L.; Zhao, K.; Shen, Y.; Shoemaker, R. K.; Rogers, C. T.; Michl, J. Tris-o-phenylenedioxycyclotriphosphazene (TPP) Inclusion Compounds Containing a Dipolar Molecular Rotor. *Cryst. Growth Des.* **2014**, *14*, 559−568.

(16) Rodríguez-Molina, B.; Pozos, A.; Cruz, R.; Romero, M.; Flores, B.; Farfán, N.; Santillan, R.; Garcia-Garibay, M. A. Synthesis and solid state characterization of molecular rotors with steroidal stators: ethisterone and norethisterone. *Org. Biomol. Chem.* **2010**, *8*, 2993−3000.

(17) Ramirez-Montes, P. I.; Ochoa, M. E.; Santillan, R.; Ramírez, D. J.; Farfán, N. Steroidal Wheel-and-Axle Host Type Molecules: Insights from Awkward Shape, Conformation, Z′ > 1 and Packing. *Cryst. Growth Des.* **2014**, *14*, 4681−4690.

(18) Frisch, M. J.; Trucks, G. W.; Schlegel, H. B.; Scuseria, G. E.; Robb, M. A.; Cheeseman, J. R.; Montgomery, J. A.; Vreven, J. T.; Kudin, K. N.; Burant, J. C.; Millam, J. M.; Iyengar, S. S.; Tomasi, J.; Barone, V.; Mennucci, B.; Cossi, M.; Scalmani, G.; Rega, N.; Petersson, G. A.; Nakatsuji, H.; Hada, M.; Ehara, M.; Toyota, K.; Fukuda, R.; Hasegawa, J.; Ishida, M.; Nakajima, T.; Hona, Y.; Kitao, O.; Nakai, H.; Klene, M.; Li, X.; Knox, J. E.; Hratchian, H. P.; Cross, J. B.; Adamo, C.; Jaramillo, J.; Gomperts, R.; Stratmann, R. E.; Yazyev, O.; Austin, A. J.; Cammi, R.; Pomelli, C.; Ochterski, J. W.; Ayala, P. Y.; Morokuma, K.; Voth, G. A.; Salvador, P.; Dannenberg, J. J.; Zakrzewski, V. G.; Dapprich, S. A.; Daniels, D.; Strain, M. C.; Farkas, O.; Malick, D. K.; Rabuck, A. D.; Raghavachari, K.; Foresman, J. B.; Ortiz, J. V.; Cui, Q.; Baboul, A. G.; Clifford, S.; Cioslowski, J.; Stefanov, B. B.; Liu, G.; Liashenko, A.; Piskorz, P.; Komaromi, I.; Martin, R. L.; Fox, D. J.; Keith, T.; Al-Laham, M. A.; Peng, C. Y.; Nanayakkara, A.; Challacombe Gill, P. M. W.; Johnson, B.; Chen, W.; Wong, M. W.; Gonzalez, C.; Pople, J. A. *Gaussian 03*, Revision B.03; Gaussian, Inc.: Pittsburgh PA, 2003.

(19) Frisch, M. J.; Trucks, G. W.; Schlegel, H. B.; Scuseria, G. E.; Robb, M. A.; Cheeseman, J. R.; Scalmani, G.; Barone, V.; Petersson, G. A.; Nakatsuji, H.; et al.*Gaussian 16*, Revision A.03; Gaussian, Inc.: Wallingford, CT, USA, 2016.

(20) Becke, A. D. Density-functional thermochemistry. III. The role of exact exchange. *J. Chem. Phys.* **1993**, *98*, 5648−5652.

(21) Frisch, M. J.; Pople, J. A.; Binkley, J. S. Self-consistent molecular orbital methods 25. Supplementary functions for Gaussian basis sets. *J. Chem. Phys.* **1984**, *80*, 3265−3269.

(22) Merrick, J. P.; Moran, D.; Radom, L. An Evaluation of Harmonic Vibrational Frequency Scale Factors. *J. Phys. Chem. A* **2007**, *111*, 11683−11700.

(23) Scott, A. P.; Radom, L. Harmonic Vibrational Frequencies: An Evaluation of Hartree−Fock, Møller−Plesset, Quadratic Configuration Interaction, Density Functional Theory, and Semiempirical Scale Factors. *J. Phys. Chem.* **1996**, *100*, 16502−16513.
(24) Sun, R.; Yao, J.; Li, S.; Gu, R. Raman spectroscopic and density functional theory studies on a benzothiazole-2-thione derivative. *Vib. Spectrosc.* **2008**, *47*, 38−43.
(25) Dennington, R.; Keith, T.; Millam, J. *GaussView*, version 5; Semichem Inc.: Shawnee Mission, KS, 2009.
(26) Jastrzębska, I.; Górecki, M.; Frelek, J.; Santillan, R.; Siergiejczyk, L.; Morzycki, J. W. Photoinduced Isomerization of 23-Oxosapogenins: Conformational Analysis and Spectroscopic Characterization of 22-Isosapogenins. *J. Org. Chem.* **2012**, *77*, 11257−11269.
(27) Frelek, J.; Butkiewicz, A.; Górecki, M.; Wojcieszczyk, R. K.; Luboradzki, R.; Kwit, M.; Rode, M. F.; Szczepek, W. J. Structure − chiroptical properties relationship of cisoidenones with an α-methylenecyclopentanone unit. *RSC Adv.* **2014**, *4*, 43977−43993.
(28) Frelek, J.; Górecki, M.; Dziedzic, A.; Jabłońska, E.; Kamieński, B.; Wojcieszczyk, R. K.; Luboradzki, R.; Szczepek, W. J. Comprehensive spectroscopic characterization of finasteride polymorphic forms. Does the form X exist? *J. Pharm. Sci.* **2015**, *104*, 1650−1657.
(29) Górecki, M.; Dziedzic, A.; Luboradzki, R.; Ostaszewska, A.; Frelek, J.; Szczepek, W. J. Synthesis and comprehensive structural and physicochemical characterization of dutasteride hydrochloride hydrate solvates. *Steroids* **2017**, *124*, 72−80.
(30) Bruhn, T.; Schaumlöffel, A.; Hemberger, Y.; Pescitelli, G. *SpecDis*, version 1.71: Berlin, Germany, 2017. Available online: https://specdis-software.jimdo.com.
(31) Woznica, M.; Kowalska, P.; Lysek, R.; Masnyk, M.; Górecki, M.; Kwit, M.; Furche, F.; Frelek, J. Stereochemical Assignment of β-lactam Antibiotics and their Analogues by Electronic Circular Dichroism Spectroscopy. *Curr. Org. Chem.* **2010**, *14*, 1022−1036.
(32) Grolik, J.; Dudek, Ł.; Eilmes, J.; Eilmes, A.; Górecki, M.; Frelek, J.; Heinrich, B.; Donnio, B. New chiral discotics with helical organization of the mesophase—liquid crystalline derivatives of dibenzotetraaza[14]annulene. *Tetrahedron* **2012**, *68*, 3875−3884.
(33) Kołodziejska, R.; Górecki, M.; Frelek, J.; Dramiński, M. Enantioselective enzymatic desymmetrization of the prochiral pyrimidine acyclonucleoside. *Tetrahedron: Asymmetry* **2012**, *23*, 683−689.
(34) Górecki, M.; Karczmarska-Wódzka, A.; Kołodziejska, R.; Dramiński, M.; Frelek, J. Determination of the Stereostructure of Pyrimidine Nucleoside Derivatives with a Combination of Various Chiroptical Methods. *Eur. J. Org. Chem.* **2014**, *43*, 5204−5213.
(35) Jeziorna, A.; Stopczyk, K.; Skorupska, E.; Luberda-Durnas, K.; Oszajca, M.; Lasocha, W.; Górecki, M.; Frelek, J.; Potrzebowski, M. J. Cyclic Dipeptides as Building Units of Nano- and Microdevices: Synthesis, Properties, and Structural Studies. *Cryst. Growth Des.* **2015**, *15*, 5138−5148.
(36) Rehman, N. U.; Hussain, H.; Al-Shidhani, S.; Avula, S. K.; Abbas, G.; Anwar, M. U.; Górecki, M.; Pescitelli, G.; Al-Harrasi, A. Incensfuran: isolation, X-ray crystal structure and absolute configuration by means of chiroptical studies in solution and solid state. *RSC Adv.* **2017**, *7*, 42357−42362.
(37) Górecki, M.; Carpita, L.; Arrico, L.; Zinna, F.; Di Bari, L. Chiroptical methods in a wide wavelength range for obtaining Ln^{3+} complexes with circularly polarized luminescence of practical interest. *Dalton Trans.* **2018**, *47*, 7166−7177.
(38) Pescitelli, G.; Bruhn, T. Good Computational Practice in the Assignment of Absolute Configurations by TDDFT Calculations of ECD Spectra. *Chirality* **2016**, *28*, 466−474.

https://dx.doi.org/10.1021/acs.jpcb.0c06464
J. Phys. Chem. B 2020, 124, 9625−9635